PHYSICAL REVIEW D **91,** 014020 (2015)

Weak interactions in top-quark pair production at hadron colliders: An update

J. H. Kühn,[1] A. Scharf,[2] and P. Uwer[3]

[1]*Institut für Theoretische Teilchenphysik, Karlsruhe Institutut of Technology (KIT), 76128 Karlsruhe, Germany*

[2]*Institut für Theoretische Physik und Astrophysik, Universität Würzburg, D-97074 Würzburg, Germany*

[3]*Institut für Physik, Humboldt-Universität zu Berlin, 12489 Berlin, Germany*

(Received 28 October 2014; published 16 January 2015)

Weak corrections for top-quark pair production at hadron colliders are revisited. Predictions for collider energies of 8 TeV, adopted to the recent LHC run, and for 13 as well as 14 TeV, presumably relevant for the next round of LHC experiments, are presented. Kinematic regions with large momentum transfer are identified, where the corrections become large and may lead to strong distortions of differential distributions, thus mimicking anomalous top-quark couplings. As a complementary case we investigate the threshold region, corresponding to configurations with small relative velocity between top and antitop quarks, which is particularly sensitive to the top-quark Yukawa coupling. We demonstrate, that nontrivial upper limits on this coupling, complementary to those recently derived by the CMS and the ATLAS collaborations, are well within reach of ongoing experiments. We, furthermore, suggest a prescription that allows the implementation of these corrections in current Monte Carlo generators. Furthermore, the weak corrections have been included in the publicly available HATHOR library. The numerical results presented in this article use the same setup as the recently calculated next-to-next-to-leading-order QCD corrections. The results can thus be combined to give the most precise theoretical predictions.

DOI: 10.1103/PhysRevD.91.014020 PACS numbers: 12.15.Lk, 14.65.Ha

I. INTRODUCTION

During the past years the determination of the top-quark mass, its couplings, production and decay rates has been pursued successfully at the Tevatron. Based on an integrated luminosity of almost 10 fb^{-1} per experiment collected by both CDF and D0 at 1.96 TeV, a sample of nearly 100 000 top-quark pairs have been produced. The analysis of these events has led, for example, to a top-quark mass determination of $M_t = 173.18 \pm 0.94$ GeV [1], corresponding to a relative error of about one half of a percent. The total production cross section $\sigma_{t\bar{t}} = 7.65 \pm 0.42$ pb [2] determined at Tevatron is in very good agreement with the theory predictions [3–14]. The same is true for the cross-section measurements performed at the LHC [15–21]. Also the $t\bar{t}$ invariant mass distribution has been measured at LHC over a wide kinematical range [22–26]. Similar to the cross-section measurements the results are in agreement with the Standard Model (SM) predictions. In contrast, surprising deviations from the theory predictions have been observed in the Tevatron experiments [27–30] by investigating the so-called charge asymmetry originally predicted 15 years ago [31,32]. (For discussions of theoretical predictions in the context of the SM see, for example, Refs. [33–37]).

Although these are already impressive achievements, expectations for top-quark physics at the LHC fly even higher. Based on integrated luminosities close to 5 fb^{-1} per experiment at 7 TeV, the top-quark mass has already been determined in a combined analysis to $M_t = 173.3 \pm 1.4$ GeV [38]. (Tevatron and LHC results combined have even led to a determination with an error below 5 permille, $M_t = 173.34 \pm 0.76$ GeV [39].) With an integrated luminosity of more than 20 fb^{-1} per experiment collected recently at 8 TeV, several million top-quark pairs per experiment have been produced. The high-energy run at 14 TeV with its expected integrated luminosity of 100 fb^{-1} will deliver about 10^8 top-quark pairs per experiment during the coming years. The LHC is, obviously, a factory of top quarks, allowing for a precise determination of their properties and their production dynamics in a large kinematic region. The large center-of-mass energy available at the LHC will thus be used to investigate top production with partonic subenergies of several TeV and thus explore the point-like nature of the heaviest of the fundamental particles. On the theoretical side precise predictions valid at the highest accessible energies are required. With the recently completed next-to-next-to-leading-order (NNLO) QCD predictions [7–10] a major step has been taken. However when it comes to ultimate precision or the highest energies weak corrections significantly affect predictions within the Standard Model. Two kinematic regions are of particular interest:

(i) Hard scattering events with partonic subenergies $\hat{s}$ and momentum transfers $|\hat{t}|$ and $|\hat{u}|$ ($\hat{s}$, $\hat{u}$ and $\hat{t}$ denote the partonic Mandelstam variables) far larger than M_t are affected by large negative corrections. These may reach nearly 20%, affecting transverse momentum

and angular distributions, and might well mimic anomalous top-quark couplings. These negative corrections—if not taken into account in the theoretical predictions—could also hide a possible rise of the cross section due to a heavy resonance.

(ii) The rate for events very close to the production threshold, with relative top-antitop velocity $\beta \leq M_H/M_t$ is enhanced by the exchange of the relatively light Higgs boson. This effect can be approximately described by a Yukawa potential and is reminiscent of Sommerfeld rescattering corrections.

Weak corrections to top-quark pair production were first studied 20 years ago [40]. The complete results, where some deficiencies were corrected and the result was given in closed analytical form, can be found in Refs. [41,42] and Refs. [43,44] for quark- and gluon-induced processes, respectively. Numerical results (which, however, differed from those presented in Refs. [43,44] and were corrected later) have been published in Ref. [45]. Purely electromagnetic corrections, which can be handled separately from the weak corrections, were evaluated in Ref. [46]. As a consequence of cancellations between the positive contributions from γg fusion and negative corrections to $q\bar{q}$ annihilation the combined effect amounts at most to -4%, if one considers p_T values as high as 1.5 TeV. The impact on the $\sqrt{\hat{s}}$ distribution remains below 1%. The details of these corrections are strongly cut dependent and we refer to Ref. [46] for details.

In the present paper we refrain from repeating the somewhat lengthy analytical formulas for the weak corrections and concentrate on the physics implications. We also update results previously obtained using modern parton distribution functions (PDFs) and the most recent values for the input parameters. In Sec. III we present a prescription which allows the combination of electroweak and next-to-leading-order (NLO) QCD corrections in the framework of current Monte Carlo generators. Subsequently, in Sec. IV, we study the impact of enhanced Yukawa couplings on the threshold behavior in more detail and contrast these potential measurements with recent experimental limits on the Higgs boson decay rate.

II. LARGE MOMENTUM TRANSFERS

Before entering the detailed numerical discussion, let us recall the basic qualitative aspects of weak corrections for the present case. With the Born amplitudes being of order α_s [Figs. 1(a)–1(d)] both for quark- and gluon-induced QCD processes, and of order α_{weak} for the lowest-order weak process [Fig. 1(e)], weak corrections start entering the cross section at loop-induced order $\alpha_s^2\alpha_{\text{weak}}$ only. The absence of an interference term between the lowest-order strong and neutral-current amplitudes in the quark-induced process, which would be of order $\alpha_s\alpha_{\text{weak}}$, follows trivially from the different color flow in the two relevant amplitudes [Figs. 1(a) and 1(e), respectively].

Sample diagrams for weak corrections to quark- and gluon-induced amplitudes using the 't Hooft-Feynman gauge are shown in Figs. 2 and 3 (ϕ and χ denote the Goldstone bosons). For gluon fusion weak effects start as corrections to the QCD-induced amplitudes.

For quark-antiquark annihilation the situation is more involved in view of a specific class of order $\alpha_s^2\alpha_{\text{weak}}$ contributions to the quark-induced processes, which must be considered separately. In this case weak and strong interactions are intimately intertwined, and corrections with virtual and real (Fig. 4) gluon emission must be combined to arrive at an infrared-finite result. The proper combination of real and virtual contributions is illustrated in Fig. 5. This issue is discussed in more detail in Ref. [41]. Only a specific combination of couplings is present in this case: the top-quark triangle in Fig. 5 is attached to two gluons with vector coupling. As long as we are interested in parity-even observables (like inclusive cross sections or p_T distributions), the light-quark coupling to the Z boson is restricted to its axial coupling g_A^q proportional to its isospin I_3^q. This, in turn, leads to a strong cancellation of this specific type of correction between u- and d-quark-induced processes. Since, furthermore, these contributions are small (see Fig IV.3 of Ref. [41]) for one species of quarks already, (less than 1% at threshold and about 2% at very high energies), this group of corrections will be neglected in the following discussion. This observation might, eventually, facilitate the combination of strong and weak corrections discussed at the end of this paper.

For large parton energies the total corrections are negative, for quark- as well as for gluon-induced processes. However, as a consequence of the nonvanishing weak charge both in the initial as well as in the final state, the corrections for quark-induced top production are about twice those of the gluon-induced process, with important consequences for the energy dependence of the corrections.

As discussed in Ref. [44] for proton-proton collisions at 14 TeV, the total cross section for top production is dominated by gluon fusion. In contrast, the production of top quarks at large transverse momenta is mainly induced by quark-antiquark annihilation, a consequence of the different parton luminosities (see Figs. 6 and 7 for LHC running at 8 TeV; results for the LHC operating at 13 or 14 TeV are shown in Figs. 16–19 in Appendix A. 2). The relative increase of the quark-induced processes in combination with the different strength of the weak corrections for the two reactions thus leads to an additional increase of weak corrections for very large transverse momenta.

For the numerical results presented in this paper we use the PDF set MSTW2008NNLO[1] [47], evaluated at a factorization scale $\mu_F = M_t$, and the coupling constants

[1]We follow closely the setup used for the NNLO QCD corrections [8–10] so that the results presented here can be directly combined.

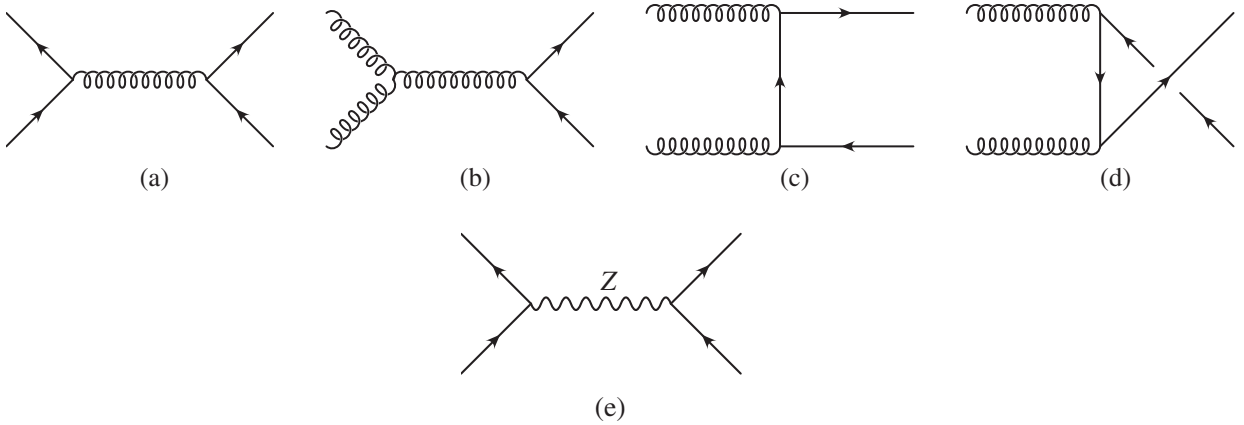

FIG. 1. Lowest-order QCD (a)–(d) and weak (e) amplitudes.

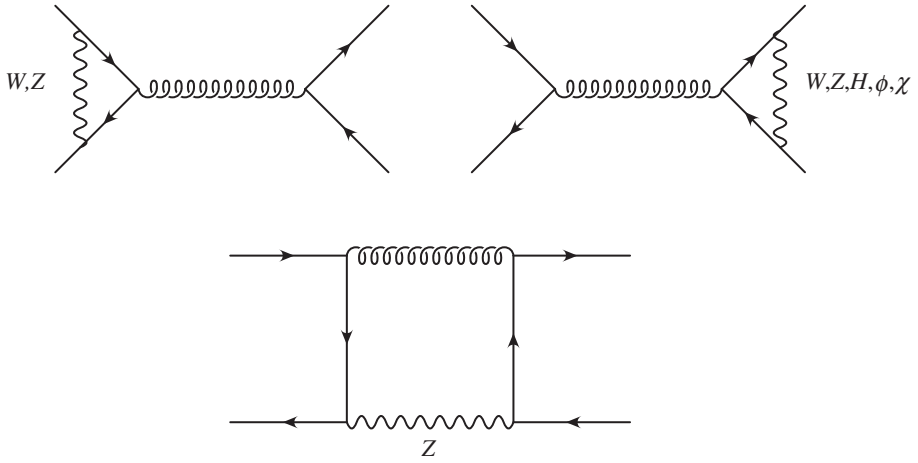

FIG. 2. Sample diagrams for the virtual corrections to the quark-induced process.

$$\alpha(M_t) = \frac{1}{127.0},$$
$$\alpha_s(M_t) = 0.106823,$$
$$\sin^2\theta_W = 1 - \frac{M_W^2}{M_Z^2}.$$

For the masses we use

$$M_Z = 91.1876\ \text{GeV}, \qquad M_W = 80.385\ \text{GeV},$$
$$M_b = 4.82\ \text{GeV}, \qquad M_t = 173.2\ \text{GeV},$$

and, if not stated otherwise, $M_H = 126$ GeV.

Another important aspect is the nontrivial angular dependence of the weak corrections. As is well known, the leading Sudakov logarithms proportional to $\log^2(s/M_W^2)$ are only dependent on the (weak) charge of the incoming and outgoing particles; subleading terms may exhibit a nontrivial angular dependence (see e.g. Refs. [48,49]). This is reflected in the characteristic angular-dependent virtual corrections which affect the rapidity distributions of top quarks at the LHC and might well mimic anomalous couplings of the particles involved.

Let us now enter the description of the corrections in more detail. The corrections at the partonic level are shown in Fig. 8 for quark- and gluon-induced processes as functions of $\hat{s}$. For the quark-antiquark channel we include only the infrared-finite vertex corrections which are responsible for the Sudakow suppression at large momentum transfer. The box contributions for the $q\bar{q}$ process are important only for the charge-asymmetric piece [33–37], and can be neglected in the present context. As expected, away from very small $\hat{s}$ the corrections are negative and about twice as large for quark- compared to gluon-induced processes. Only very close to threshold does one observe corrections which become positive for a light Higgs boson and these will be discussed in Sec. III. For the ficticious case of $M_H = 1$ TeV two pronounced structures are visible in the gluon-fusion channel: the interference between the Born amplitude and the s-channel Higgs boson contribution (last diagram of Fig. 3) is visible as slight depletion

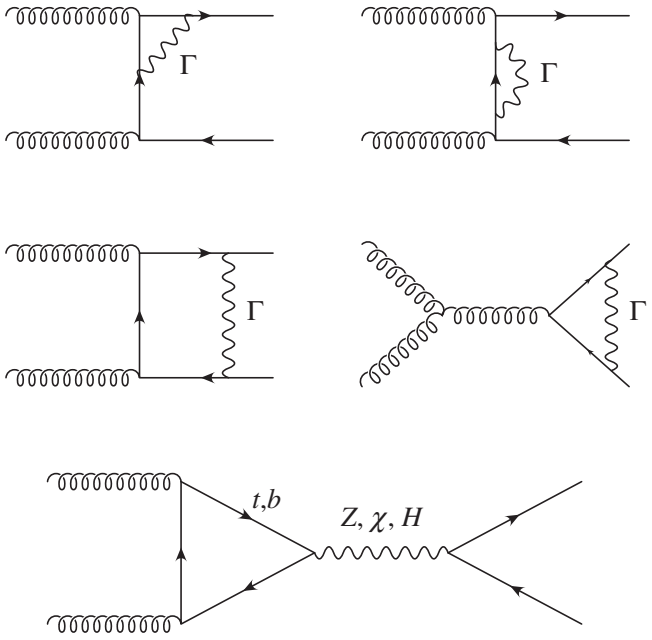

FIG. 3. Sample diagrams for the virtual corrections for the gluon-induced process. Γ stands for all contributions from the gauge boson, Goldstone boson and Higgs exchange.

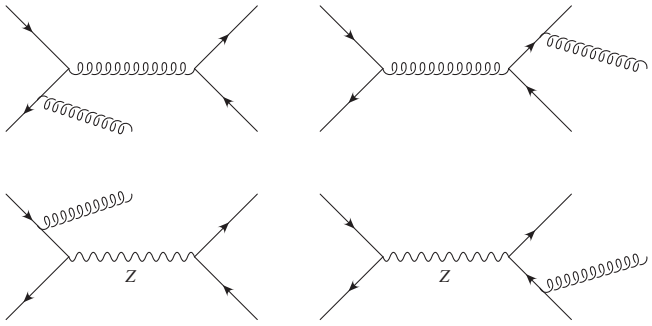

FIG. 4. Sample diagrams for the real corrections to the quark-induced process.

around 1 TeV; the interference with the Z plus χ contribution arising from the same diagram is responsible for the dip close to the threshold. For $M_H = 126$ GeV this dip is overcompensated by the positive contribution of roughly 5% from the Yukawa interaction discussed in more detail in Sec. III. This same difference of 5% between $M_H = 126$ GeV and 1 TeV is also visible in the threshold behavior of the $q\bar{q}$-initiated reaction.

The angular dependence of the corrections is shown in Fig. 9 separately for quark- and gluon-induced processes close to threshold at 370 GeV (upper solid blue curve) and for 3 TeV (lower dotted red line). Let us, in a first step, discuss the results for the quark-induced reaction (Fig. 9 left). Again we restrict the analysis to the vertex correction. Close to threshold the process is dominated by (isotropic) S waves, while at high energies (3 TeV) the Dirac form factor dominates both for the Born amplitude and the correction. This leads to a constant ratio as a function of the scattering angle. At low energies ($\sqrt{\hat{s}} = 370$ GeV) we find a positive correction of about 2%. At large energies, say $\sqrt{\hat{s}} = 3$ TeV, the Sudakow suppression leads to negative corrections of about −18%. Note that the box diagrams while not particularly enhanced would lead to sizable asymmetric and small symmetric corrections. For details we refer to Ref. [35]. The gluon-induced part, in contrast, is markedly angular dependent. For large $\hat{s}$ and small scattering angle the corrections are small, since the Sudakov-like behavior cannot be expected in this case. At 90 degrees, in contrast, the Sudakov limit is applicable and the corrections become large. Let us now discuss observables at the hadron level. As opposed to the discussion at parton level we now also include box contributions and real corrections in the analysis, and thus the full set of corrections are investigated. The corrections for the total cross section are shown in Fig. 10 as function of $\sqrt{s}$, for two characteristic choices of the Higgs mass, $M_H = 126$ GeV and 1000 GeV. We allow M_H to move away from its recently determined value to illustrate the effect of the Higgs-top Yukawa coupling. The corrections are evidently small, of order −2% for all LHC energies and are only moderately sensitive to M_H. Given the recent progress concerning the NNLO QCD calculations the theoretical uncertainties will eventually reach 3–4%. At this level of accuracy the weak corrections become important and need to be taken into account. As a reference we show in Fig. 11 the weak correction as a function of the top-quark mass. At a center-of-mass energy of 8 TeV the corrections are about −1.85%. At 14 TeV the high-energy regime of the cross section becomes more accessible leading to slightly larger corrections of the order of

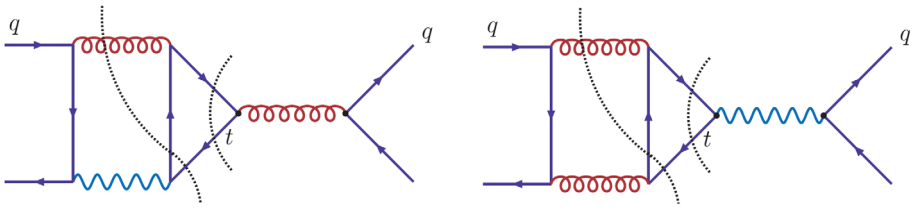

FIG. 5 (color online). Sample diagrams for the proper combination of virtual and real corrections to the quark-induced process. The dotted lines show different cuts corresponding to virtual and real corrections.

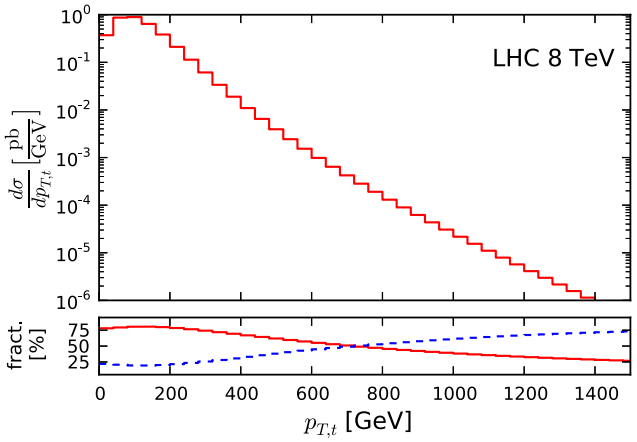

FIG. 6 (color online). Leading-order differential cross section for the LHC (8 TeV) as a function of p_T. The lower plot shows the fraction from gluon fusion (red, solid) and the fraction from quark-antiquark annihilation (blue, dashed).

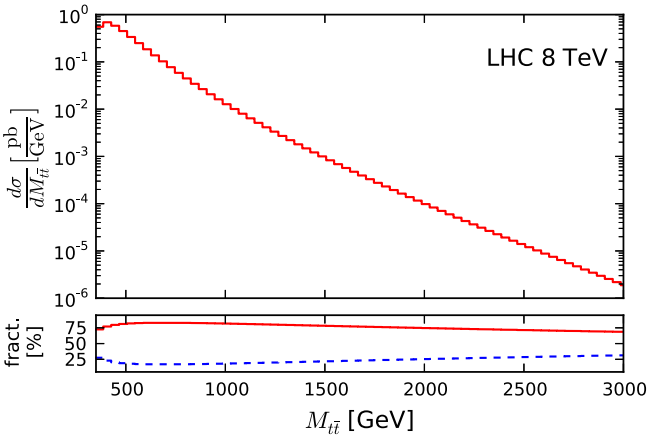

FIG. 7 (color online). Leading-order differential cross section for the LHC (8 TeV) as a function of $M_{t\bar{t}}$. The lower plot shows the fraction from gluon fusion (red, solid) and the fraction from quark-antiquark annihilation (blue, dashed).

−2.0%. For convenience we provide a parametrization for the weak corrections valid for $172.4 < M_t < 174$:

$$\delta\sigma_{\text{EW}}^{8\,\text{TeV}} = -2.69\ \text{pb} + 0.06\ \text{pb} \times (M_t/\text{GeV} - 173.2), \quad (1)$$

$$\delta\sigma_{\text{EW}}^{13\,\text{TeV}} = -9.48\ \text{pb} + 0.20\ \text{pb} \times (M_t/\text{GeV} - 173.2), \quad (2)$$

$$\delta\sigma_{\text{EW}}^{14\,\text{TeV}} = -11.30\ \text{pb} + 0.23\ \text{pb} \times (M_t/\text{GeV} - 173.2). \quad (3)$$

As can be seen from Fig. 11 and the parametrization above, the mass dependence is very small in the range 172.4–174 GeV and can be neglected for most phenomenological applications. The aforementioned results can be directly combined with NNLO results calculated using the MSTW2008NNLO PDF set [47]. Since ratios are more robust with respect to different choices for the parton distribution functions we also present a parametrization for the relative corrections:

$$\frac{\delta\sigma_{\text{EW}}^{8\,\text{TeV}}}{\sigma_{\text{LO}}} = -1.85\% - 0.01\% \times (M_t/\text{GeV} - 173.2), \quad (4)$$

$$\frac{\delta\sigma_{\text{EW}}^{13\,\text{TeV}}}{\sigma_{\text{LO}}} = -2.00\% - 0.01\% \times (M_t/\text{GeV} - 173.2), \quad (5)$$

$$\frac{\delta\sigma_{\text{EW}}^{14\,\text{TeV}}}{\sigma_{\text{LO}}} = -2.01\% - 0.01\% \times (M_t/\text{GeV} - 173.2). \quad (6)$$

Note that the coupling constants of the strong interactions cancel in the ratios. In addition, for the ratios the mass dependence is further reduced and completely negligible in the range 172.4–174 GeV. One may argue that some contributions of the QCD corrections are universal and will also correct the weak contributions (see also the discussion in Sec. III). Based on this assumption one may use

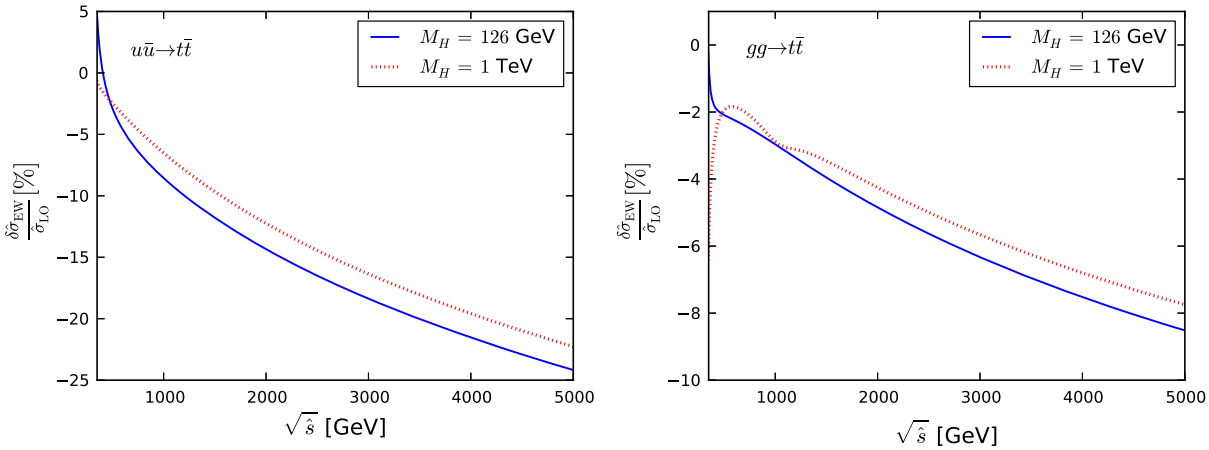

FIG. 8 (color online). Relative weak corrections at parton level for the quark- and gluon-induced reactions as functions of the squared parton energy $\hat{s}$ for two characteristic masses of the Higgs boson.

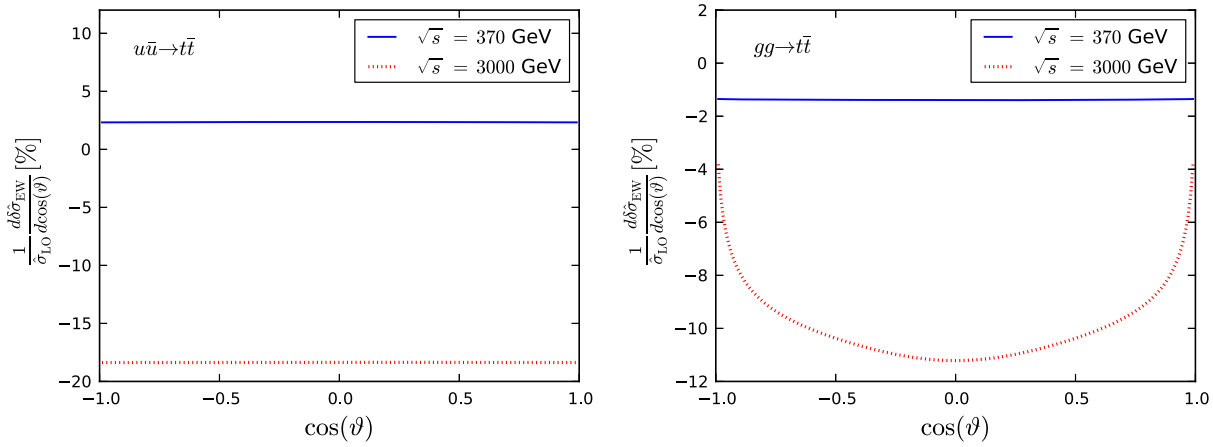

FIG. 9 (color online). Relative weak corrections for the quark- and gluon-induced reactions as functions of the scattering angle close to threshold ($\sqrt{\hat{s}} = 370$ GeV, solid line) and at high energies ($\sqrt{\hat{s}} = 3$ TeV, dotted line).

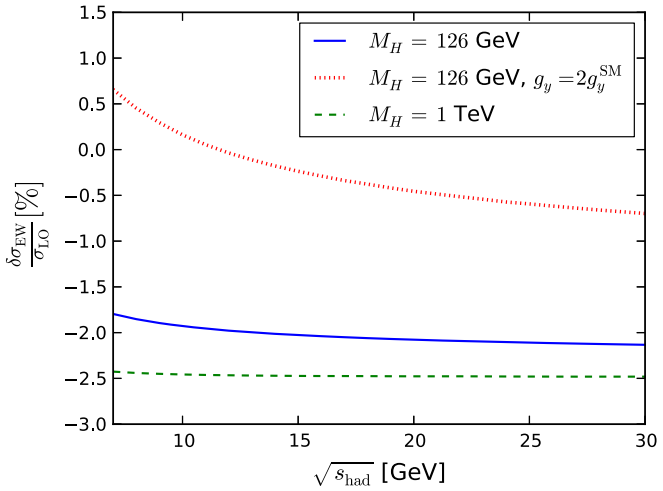

FIG. 10 (color online). Relative weak corrections for the total cross section as functions of the total center-of-mass energy for two different masses of the Higgs boson and for a rescaled Yukawa coupling.

$$\delta\sigma_{\rm EW} = \frac{\delta\sigma_{\rm EW}}{\sigma_{\rm LO}} \times \sigma_{\rm NNLO}^{\rm QCD} \tag{7}$$

to estimate the size of the weak corrections. For $M_t = 173.2$ GeV this leads to

$$\delta\sigma_{\rm EW}^{8\,\rm TeV} = -4.4\ \text{pb}, \tag{8}$$

$$\delta\sigma_{\rm EW}^{13\,\rm TeV} = -15.8\ \text{pb}, \tag{9}$$

$$\delta\sigma_{\rm EW}^{14\,\rm TeV} = -18.8\ \text{pb}. \tag{10}$$

In addition we demonstrate in Fig. 10 the impact of an enhanced Yukawa coupling with $g_Y = 2g_Y^{\rm SM}$. In this case the negative corrections from the large transverse momentum region are overcompensated by the positive ones for small $t\bar{t}$ masses. Let us emphasize that such an analysis might well lead to a nontrivial limit on the top-quark Yukawa coupling g_Y. The weak corrections have a trivial dependence on the Yukawa coupling. A large fraction of

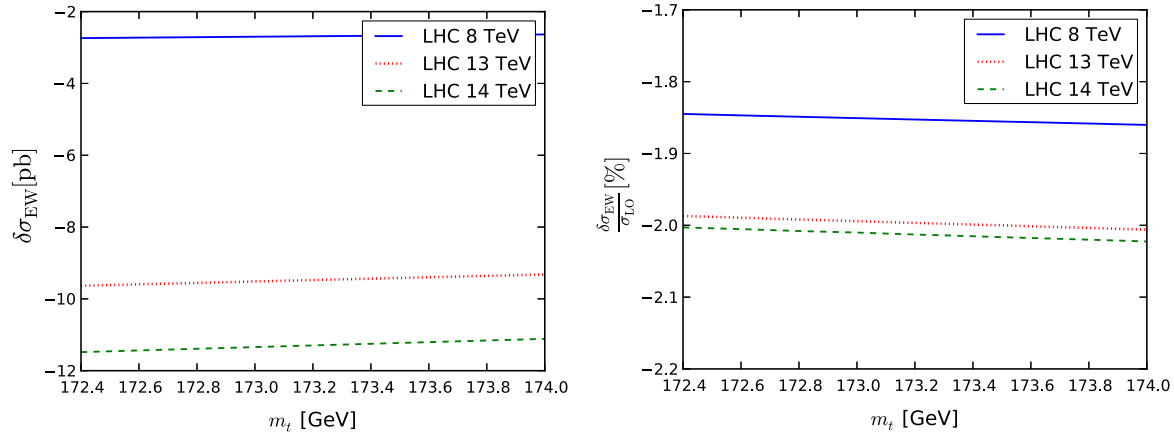

FIG. 11 (color online). Weak corrections as function of the top-quark mass.

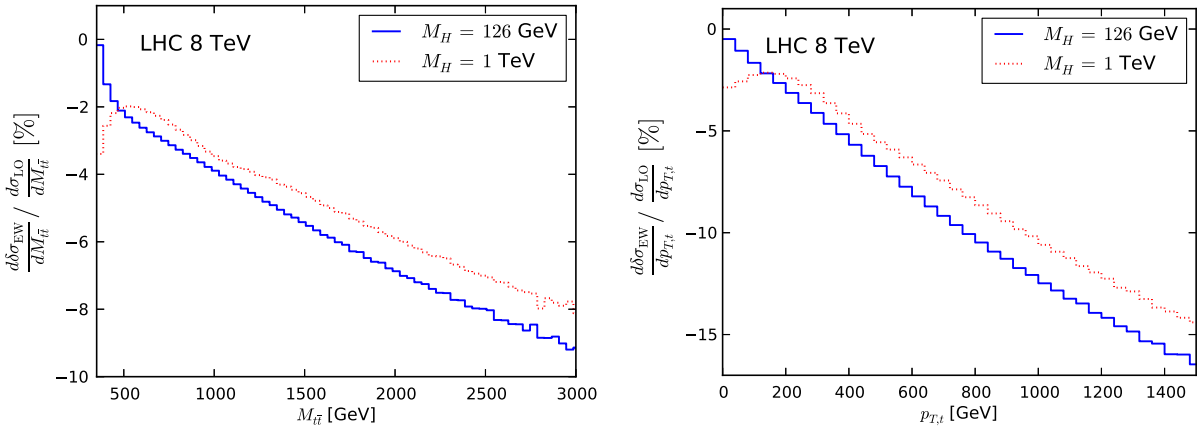

FIG. 12 (color online). Relative weak corrections for the invariant $t\bar{t}$ mass (left) and transverse momentum (right) distributions for the LHC for Higgs masses of 126 GeV and 1 TeV.

the corrections does not depend on g_Y. The production of an intermediate s-channel Higgs boson through a closed b-quark loop leads to a contribution linear in the top-quark Yukawa coupling. Due to the small b-quark mass, this contribution is expected to be very small. The remaining dependence on the top-quark Yukawa coupling is quadratic, since it always involves two $Ht\bar{t}$ vertices. For the total cross section we find the following parametric dependence ($M_t = 173.2$ GeV):

$$\delta\sigma_{\rm EW}^{8\,\rm TeV} = (-3.80 + 0.0009 g_Y + 1.12 g_Y^2)\ \text{pb}, \quad (11)$$

$$\delta\sigma_{\rm EW}^{13\,\rm TeV} = (-12.47 + 0.0136 g_Y + 2.99 g_Y^2)\ \text{pb}, \quad (12)$$

$$\delta\sigma_{\rm EW}^{14\,\rm TeV} = (-14.74 + 0.0146 g_Y + 3.45 g_Y^2)\ \text{pb}. \quad (13)$$

Indeed we observe that the linear dependence on g_Y is very weak and can be neglected as anticipated above. Again it might be useful to study the size of the relative corrections:

$$\frac{\delta\sigma_{\rm EW}^{8\,\rm TeV}}{\sigma_{\rm LO}} = (-2.62 + 0.0006 g_Y + 0.77 g_Y^2)\%, \quad (14)$$

$$\frac{\delta\sigma_{\rm EW}^{13\,\rm TeV}}{\sigma_{\rm LO}} = (-2.63 + 0.0029 g_Y + 0.63 g_Y^2)\%, \quad (15)$$

$$\frac{\delta\sigma_{\rm EW}^{14\,\rm TeV}}{\sigma_{\rm LO}} = (-2.63 + 0.0026 g_Y + 0.61 g_Y^2)\%. \quad (16)$$

A shift of g_Y by a factor of 3 would enhance the cross section by about 5% and might thus become experimentally accessible. As discussed in Sec. IV, this limit can be further improved by restricting the sample to events close to the production threshold.

While for the total cross section the weak corrections are small, the situation is drastically different, once we consider differential distributions in the region of large transverse momenta $p_{\rm T}$ or large masses $M_{t\bar{t}}$ of the $t\bar{t}$ system where Sudakov logarithms start to play an important role. The corrections are shown in Fig. 12 for proton-proton collisions at a center-of-mass energy of 8 TeV both for the $p_{\rm T}$

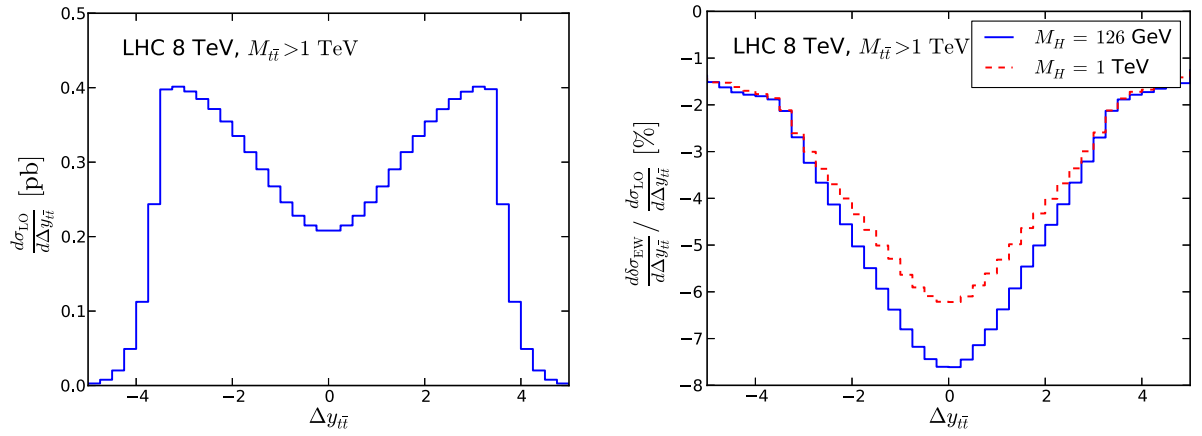

FIG. 13 (color online). Rapidity distributions with invariant mass cuts at leading order (left) and relative weak corrections (right).

and the $M_{t\bar{t}}$ distributions. (Results for 13 and 14 TeV are shown in Figs. 20 and 21 in Appendix A. 2.) For illustration we present again the relative corrections for Higgs masses of 126 GeV and 1 TeV. The strong increase with increasing p_T is evident. Based on the present data sample, corresponding to more than 20 fb^{-1}, corrections close to -10% could be observed at $\sqrt{s} = 8$ TeV if events with top quarks of large transverse momenta, say 750 GeV, are considered.

To investigate the angular dependence of the $t\bar{t}$ system in its center-of-mass frame one could consider the distribution in the rapidity difference $\Delta y_{t\bar{t}} = y_t - y_{\bar{t}}$ which, for fixed $M_{t\bar{t}}$ can be directly translated into the angular distribution. To illustrate the distributions and the size of the corrections, the differential distributions $d\sigma/d\Delta y_{t\bar{t}}$ are shown in Fig. 13 for 8 TeV, considering only events with $M_{t\bar{t}}$ larger than 1 TeV. (For 13 and 14 TeV the results are shown in Figs. 22 and 23 in the Appendix.) The corresponding relative corrections are also displayed in Fig. 13. The pronounced peaking of the cross section for large rapidity differences in Fig. 13 (left) is an obvious consequence of the t-channel singularity, while the enhanced negative corrections around $\Delta y_{t\bar{t}} = 0$ in Fig. 13 (right) are a consequence of the Sudakov condition $\hat{s}$ and $|\hat{t}| \gg M_W^2$. Since the distribution in $\Delta y_{t\bar{t}}$ is at the same time sensitive to anomalous couplings, these could well be masked by the large radiative corrections.

III. QCD AND ELECTROWEAK CORRECTIONS COMBINED

Let us at this point speculate about the combination of weak and QCD corrections. Clearly, the evaluation of corrections of $\mathcal{O}(\alpha_s\alpha)$ is out of reach in the foreseeable future. Thus, strictly speaking, both multiplicative [of the form $(1+\delta_{\rm QCD})(1+\delta_W)$] and additive [of the form $(1+\delta_{\rm QCD}+\delta_W)$] treatments are equally justified. The difference between the two assumptions can be considered as an estimate of the theoretical uncertainties. It may be useful, however, to devise a strategy to eventually implement the major part of the combined corrections. As mentioned in the beginning, QED and purely weak corrections can be treated separately in the present case. Furthermore, QED corrections are small and the resulting uncertainty of combined QCD and QED terms is even smaller. In principle, by adjusting color coefficients, the recently available two-loop QCD corrections [8–10] could be employed to arrive at the full combined QED and QCD results. Concerning the weak corrections, we observe that a major part of the QCD corrections originates from configurations involving soft and/or collinear emission. Let us then reconstruct the effective two-body kinematics by using the $t\bar{t}$ invariant mass as $\hat{s}$ and the scattering angle with respect to the beam direction, as defined in the $t\bar{t}$ rest frame as the partonic scattering angle. Using this information would allow us to apply the weak correction factor which also depends on $\hat{s}$ and $\hat{t}$ only.

Let us describe the prescriptions in more detail. As discussed before, the corrections depicted in Figs. 4 and 5 can be ignored. Three overall correction factors $K_{u\bar{u}}$, $K_{d\bar{d}}$ and K_{gg} with

$$K_{ij} = \frac{d\sigma_{ij}^{\rm EW}/d\cos(\theta)}{d\sigma_{ij}^{\rm LO}/d\cos(\theta)}$$

remain, which are for given M_H, M_W and M_Z functions of $\hat{s}$ and $\hat{t}$ and are appropriate for the three basic two-to-two processes. Numerical results for the $K_{u\bar{u}}$ and K_{gg} are shown in Fig. 9 with $\sqrt{\hat{s}}$ fixed to 370, and 3000 GeV. We have implemented the corresponding analytic formulas in the publicly available HATHOR program [4,50] version 2.1 which is available at http://www.physik.hu-berlin.de/pep/tools/hathor.html. The correction factors for u and d quarks are nearly the same and angular independent; the correction factor for the gluon-induced process is most pronounced for top quarks produced in the transverse direction.

It is important to keep in mind that the corrections do not affect the two-to-two kinematics. This allows us to implement the electroweak corrections into any Monte Carlo generator for $t\bar{t}$ production as follows. In a first step we consider a generator which does not involve NLO QCD corrections. The invariant mass of the $t\bar{t}$ system will be identified with $\sqrt{\hat{s}}$. Let us now denote the directions of the momenta of top and antitop quarks in the $t\bar{t}$ rest frame by $\vec{\mathbf{e}}_{\mathbf{t}}^{\,*}$ and $\vec{\mathbf{e}}_{\bar{\mathbf{t}}}^{\,*}$, respectively, the directions of the beam momenta by $\vec{\mathbf{e}}_{\mathbf{1}}^{\,*}$ and $\vec{\mathbf{e}}_{\mathbf{2}}^{\,*}$, the direction of the effective scattering axis by[2]

$$\hat{\vec{\mathbf{e}}}^{\,*} \equiv \frac{\vec{\mathbf{e}}_{\mathbf{1}}^{\,*} - \vec{\mathbf{e}}_{\mathbf{2}}^{\,*}}{|\vec{\mathbf{e}}_{\mathbf{1}}^{\,*} - \vec{\mathbf{e}}_{\mathbf{2}}^{\,*}|} \tag{17}$$

and the effective scattering angle by

$$\cos\theta^* \equiv \vec{\mathbf{e}}_{\mathbf{t}}^{\,*} \cdot \hat{\vec{\mathbf{e}}}^{\,*}. \tag{18}$$

The partonic variables are thus obtained from

$$\hat{s} \equiv M_{t\bar{t}}^2, \qquad \hat{t} \equiv m_t^2 - \frac{\hat{s}}{2}\left(1 - \sqrt{1 - \frac{4m_t^2}{\hat{s}}}\cos\theta^*\right). \tag{19}$$

Inspecting the event, as generated through the program, more closely, it can be assigned in a unique way to the $u\bar{u}$-, $d\bar{d}$- or gg-induced subprocess. Using the correction functions $K_i(\hat{s},\hat{t})$ with $i = u\bar{u}$, $d\bar{d}$ or gg, the reweighting can be performed in a straightforward way.

The kinematic prescription outlined above can also be applied to generators which include NLO QCD corrections. Events which involve collinear or soft quark or gluon emission are responsible for the major part of QCD corrections. For these events one would expect that the dominant weak corrections can still be derived from the

[2]This approach follows the one introduced in Ref. [51] for gauge-boson pair production.

same correction functions with $\hat{s}$ and $\hat{t}$ as derived from Eq. (19) above. For final states with the $t\bar{t}$ system produced at large transverse momentum, balanced by a hard quark or gluon jet at large P_t, our prescription will no longer properly account for the electroweak corrections. However, the missing terms are of order $\alpha_s\alpha_{\text{weak}}$ and their evaluation would require the electroweak corrections for the full set of two-to-three reactions.

It remains to assign the proper correction function K_i for the full set of partonic processes. For the subprocesses $q\bar{q} \to t\bar{t}(g)$ and $gg \to t\bar{t}(g)$ the functions $K_{q\bar{q}}$ and K_{gg} will be employed. The assignment of correction factors to the reaction $qg \to t\bar{t}q$ (and its charge conjugate) is more involved. Let us assume that the incoming quark originates from hadron 1 and splits into a nearly collinear quark and gluon. The latter fuses with the gluon from hadron 2 into $t\bar{t}$. In this case the factor K_{gg} is suggested. Alternatively one may consider a situation where the incoming gluon splits into a nearly collinear $q\bar{q}$ pair, with the antiquark annihilating into $t\bar{t}$. In this case the use of $K_{q\bar{q}}$ seems more adequate.

To distinguish the two options, we consider the scattering angle θ_q of the outgoing quark relative to hadron 1 in the $t\bar{t}$ rest frame. If $0 \le \theta_q < \pi/2$, we take K_{gg}; if $\pi/2 \le \theta_q < \pi$, we take $K_{q\bar{q}}$. In the limiting cases of nearly collinear emission this convention leads to the desired result, while in the case of events with a quark jet at large transverse momentum the expected error will be of order $\alpha_s\alpha_{\text{weak}}$.

An alternative method to define a reduced kinematics in the case of additional emission could be to use a boost similar to what has been done in the matrix element method. The sensitivity to the specific prescription could be estimated by comparing the two different approaches.

IV. THE TOP-PAIR THRESHOLD REGION AND THE YUKAWA COUPLING

As illustrated in Fig. 8, the corrections for top-pair production very close to threshold exhibit a significant dependence on the mass of the Higgs boson. In fact, for both quark- and gluon-induced processes the difference in the correction between a light ($M_H = 126$ GeV) and a heavy ($M_H = 1000$ GeV) Higgs boson amounts to about 5%. This effect has been discussed in some detail for pair production at an electron-positron collider [53–57] and for quark-antiquark collisions [57] and is closely related to the well-known Sommerfeld rescattering corrections, originally obtained in the framework of QED. Similar considerations are also applicable to gluon fusion [44].

For a Yukawa potential induced by the Higgs exchange,

$$V_Y(r) = -\kappa\frac{1}{r}e^{-r/r_Y} \quad \text{with}$$
$$\kappa = \frac{g_Y^2}{4\pi} = \frac{\sqrt{2}G_F M_t^2}{4\pi} \approx 0.0337 \quad \text{and} \quad r_Y = 1/M_H, \tag{20}$$

the dominant correction evaluated directly at threshold is given by the factor $1 + \kappa\frac{M_t}{M_H}$. (The full result including the energy dependence, can be found in Refs. [53,56].) Indeed the difference of 5% between the heavy and the light Higgs boson is well consistent with this simple approximation. For quark-antiquark annihilation the positive offset is shown in Fig. 8 (left). For gluon fusion the Yukawa enhancement is partially masked by a negative contribution originating from the interference of the tree-level amplitude with the amplitude from the triangle diagrams with Z and χ in the s channel (Fig. 3). The difference, however, between a heavy and a light Higgs boson of about 5% remains unchanged.

As evident from Fig. 8, the Yukawa enhancement is located in the region close to threshold, with a relative $t\bar{t}$ velocity β less than M_H/M_t. For the moment we consider the weak corrections as an overall β-dependent factor which multiplies the complicated threshold behavior induced by the partly attractive, partly repulsive QCD potential. (For QCD effects see e.g. Ref. [52] and references therein.) In principle the effect of a light Higgs exchange could be split into a short-range piece, which leads to a β-independent correction term, and a long-range piece, which can be absorbed by adding Yukawa and QCD potentials. The energy dependence can then be obtained from a Green's-function treatment. This approach has been discussed in more detail in Ref. [57] for the cases of top production in electron-positron and quark-antiquark annihilation. Since r_Y, the characteristic length of the Yukawa potential, is still significantly smaller than r_B, the Bohr radius of the would-be toponium ground state,

$$r_Y/r_B = \left(\frac{4}{3}\alpha_s\frac{M_t}{2}\right)/M_H \approx 1/6, \tag{21}$$

the simple multiplicative treatment advocated above is sufficient for the presently required level of precision.

As discussed above, the impact on the total cross section from the variation of M_H is relatively small, less than 1%, both for the Tevatron and the LHC, and even an enhancement of the Yukawa coupling by a factor of 2 will be hardly visible. Differential distributions, however, are significantly more sensitive to the Yukawa coupling. This is demonstrated in Figs. 14 and 15, where the correction factors for the distribution with respect to $M_{t\bar{t}}$ are evaluated for the LHC at 8 TeV and the Tevatron in the region close to threshold. (Results for 13 and 14 TeV are shown in Figs. 24 and 25 in the Appendix.)

As expected from the previous discussion, differences around 5% between the cases $M_H = 126$ GeV and 1 TeV are visible. It remains to be seen, whether the experimental mass resolution and normalization of the cross section will be sufficiently precise to pin down the 5% effect and

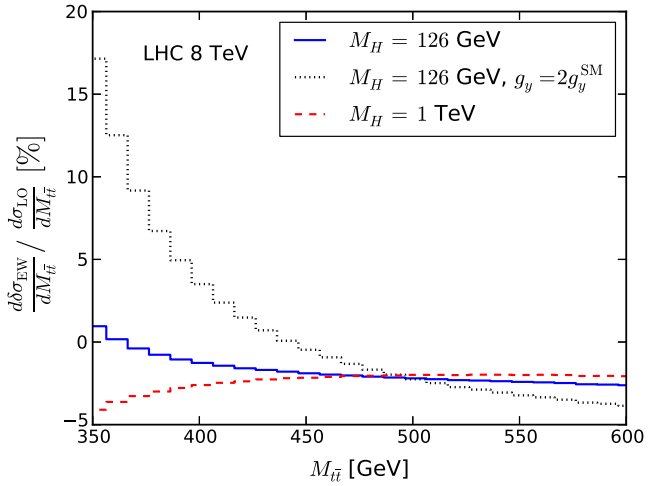

FIG. 14 (color online). Relative weak corrections for the mass distribution in the framework of the SM assuming $M_H = 126$ GeV (solid blue curve) and 1000 GeV (dashed red curve), and for the case of an enhanced Yukawa coupling $g_Y = 2g_Y^{\rm SM}$ with $M_H = 126$ GeV (dotted black curve).

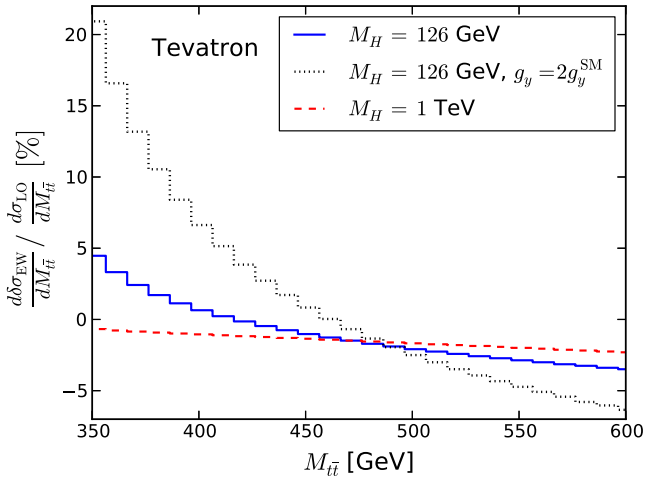

FIG. 15 (color online). Same as Fig. 14 but for the Tevatron.

thus directly determine the Yukawa coupling g_Y. At the same time this approach requires a detailed theoretical understanding of the QCD predictions for the threshold behavior, governed by the remnants of the bound states, as discussed in Ref. [52]. However, in any case this approach should allow us to provide an upper limit on modifications of g_Y that might be postulated in theories beyond the Standard Model.[3]

Let us assume, for example, the case of an enhanced Yukawa coupling $g_Y = 2g_Y^{\rm SM}$. This magnifies the Yukawa correction by a factor of 4 and implies an enhancement of the cross section close to threshold by about 20% (see dashed curves in Figs. 14 and 15). Such an energy-dependent offset relative to the SM prediction should be visible in the Tevatron or LHC analyses. To elaborate on this point further it is again useful to study the parametric dependence of the threshold cross section with respect to g_Y similar to what has been done in Sec. II for the inclusive cross section. By restricting the cross section to the threshold region by introducing a cut on the invariant mass of the top-quark pair we find for the LHC

$$\delta\sigma_{\rm EW}^{8\,\rm TeV}(m_{t\bar{t}} < 2M_t + 50\ \text{GeV}) = (-0.10 + 0.09g_Y^2)\ \text{pb}, \tag{22}$$

$$\delta\sigma_{\rm EW}^{8\,\rm TeV}(m_{t\bar{t}} < 2M_t + 100\ \text{GeV}) = (-0.19 + 0.13g_Y^2)\ \text{pb}, \tag{23}$$

$$\delta\sigma_{\rm EW}^{8\,\rm TeV}(m_{t\bar{t}} < 2M_t + 150\ \text{GeV}) = (-0.24 + 0.13g_Y^2)\ \text{pb}. \tag{24}$$

Note that we neglected the tiny contribution linear in g_Y since it is irrelevant for the phenomenology. For the relative corrections we find

$$\frac{\delta\sigma_{\rm EW}^{8\,\rm TeV}}{\sigma_{\rm LO}}(m_{t\bar{t}} < 2M_t + 50\ \text{GeV}) = (-3.53 + 3.14g_Y^2)\%, \tag{25}$$

$$\frac{\delta\sigma_{\rm EW}^{8\,\rm TeV}}{\sigma_{\rm LO}}(m_{t\bar{t}} < 2M_t + 100\ \text{GeV}) = (-3.05 + 2.05g_Y^2)\%, \tag{26}$$

$$\frac{\delta\sigma_{\rm EW}^{8\,\rm TeV}}{\sigma_{\rm LO}}(m_{t\bar{t}} < 2M_t + 150\ \text{GeV}) = (-2.83 + 1.54g_Y^2)\%. \tag{27}$$

Results for 13 and 14 TeV collider energies are given in Eqs. A1–A12 in Appendix A. 1. Using $m_{t\bar{t}} < 2M_t + 50$ GeV we see, that doubling the Yukawa coupling would lead to a change of the cross section of about 9%. As expected, restricting the cross section to the threshold region significantly enhances the sensitivity to the top-quark Yukawa coupling. Assuming an experimental precision of 5% the top-quark Yukawa coupling can be constrained. The relevance of such a limit on g_Y can be illustrated by comparing it with the limits on the Higgs couplings as suggested in Refs. [60,61] and presented recently by both the CMS [62] and ATLAS [63] collaborations. In these papers it has been demonstrated that a universal rescaling $g^{\rm SM} \to \kappa g^{\rm SM}$ combined with an increase of the Higgs width by a factor κ^4 (e.g. through some presently invisible mode) can be excluded for values of κ^4 exceeding 7.7 [63] or even 5.4 [62]. Such a rescaling would also involve the top-quark Yukawa coupling, and it remains to be seen, if similar limits can be

[3]For examples where this has been discussed in the framework of a two-Higgs-doublet model see e.g. Refs. [58,59].

obtained from an analysis of the top-quark threshold behavior.

V. OUTLOOK AND CONCLUSIONS

A sizable data sample has been collected by LHC experiments at a center-of-mass energy of 8 TeV, and the Higgs boson has been discovered with a mass of about 126 GeV [64,65]. In view of these developments an update of the weak corrections to top-quark pair production has been presented. We demonstrated that these corrections start to become important already for the 8 TeV run, if an experimental precision of 5% can be reached. This observation applies both for large transverse momenta, say above 500 GeV, where negative corrections around 5% are observed, and for top-quark production close to threshold which is enhanced by about 5% due to the attractive Yukawa interaction. A detailed study of the top-antitop spectrum close to threshold could, therefore, determine the strength of the Yukawa coupling or, at least provide interesting upper limits. We also investigated the distribution of top and antitop quarks with respect to their rapidity difference $\Delta y_{t\bar{t}}$ for the subsample with large invariant mass and observed marked distortions of order 8% (LHC8) and 12% (LHC14). Clearly these effects might be misinterpreted as evidence for anomalous couplings and thus have to be well under control. Last but not least we indicated a possible approach for combining QCD and weak corrections in the framework of a Monte Carlo generator.

ACKNOWLEDGMENTS

The work of J. H. K. was supported by the German Federal Ministry of Education and Research (BMBF) Project No. 05H12VKE. Discussions with Jeannine Wagner-Kuhr on experimental issues are gratefully acknowledged. The work of P. U. was supported by BMBF Project No. 05H12KHE. The work of A. S. has been partly supported by BMBF Project No. 05H12WWE.

APPENDIX: RESULTS FOR LHC OPERATING AT 13 OR 14 TEV

1. Parametrization of the 13 and 14 TeV cross section as a function of the top-quark Yukawa coupling

$$\delta\sigma_{\mathrm{EW}}^{13\,\mathrm{TeV}}(m_{t\bar{t}} < 2M_t + 50\ \mathrm{GeV}) = (-0.309 + 0.25 g_Y^2)\ \mathrm{pb}, \tag{A1}$$

$$\delta\sigma_{\mathrm{EW}}^{13\,\mathrm{TeV}}(m_{t\bar{t}} < 2M_t + 100\ \mathrm{GeV}) = (-0.572 + 0.36 g_Y^2)\ \mathrm{pb}, \tag{A2}$$

$$\delta\sigma_{\mathrm{EW}}^{13\,\mathrm{TeV}}(m_{t\bar{t}} < 2M_t + 150\ \mathrm{GeV}) = (-0.752 + 0.38 g_Y^2)\ \mathrm{pb}, \tag{A3}$$

$$\delta\sigma_{\mathrm{EW}}^{14\,\mathrm{TeV}}(m_{t\bar{t}} < 2M_t + 50\ \mathrm{GeV}) = (-0.360 + 0.29 g_Y^2)\ \mathrm{pb}, \tag{A4}$$

$$\delta\sigma_{\mathrm{EW}}^{14\,\mathrm{TeV}}(m_{t\bar{t}} < 2M_t + 100\ \mathrm{GeV}) = (-0.669 + 0.41 g_Y^2)\ \mathrm{pb}, \tag{A5}$$

$$\delta\sigma_{\mathrm{EW}}^{14\,\mathrm{TeV}}(m_{t\bar{t}} < 2M_t + 150\ \mathrm{GeV}) = (-0.879 + 0.44 g_Y^2)\ \mathrm{pb}. \tag{A6}$$

The relative corrections are given by

$$\frac{\delta\sigma_{\mathrm{EW}}^{13\,\mathrm{TeV}}}{\sigma_{\mathrm{LO}}}(m_{t\bar{t}} < 2M_t + 50\ \mathrm{GeV}) = (-3.753 + 3.08 g_Y^2)\%, \tag{A7}$$

$$\frac{\delta\sigma_{\mathrm{EW}}^{13\,\mathrm{TeV}}}{\sigma_{\mathrm{LO}}}(m_{t\bar{t}} < 2M_t + 100\ \mathrm{GeV}) = (-3.177 + 1.97 g_Y^2)\%, \tag{A8}$$

$$\frac{\delta\sigma_{\mathrm{EW}}^{13\,\mathrm{TeV}}}{\sigma_{\mathrm{LO}}}(m_{t\bar{t}} < 2M_t + 150\ \mathrm{GeV}) = (-2.908 + 1.45 g_Y^2)\%, \tag{A9}$$

$$\frac{\delta\sigma_{\mathrm{EW}}^{14\,\mathrm{TeV}}}{\sigma_{\mathrm{LO}}}(m_{t\bar{t}} < 2M_t + 50\ \mathrm{GeV}) = (-3.775 + 3.08 g_Y^2)\%, \tag{A10}$$

$$\frac{\delta\sigma_{\mathrm{EW}}^{14\,\mathrm{TeV}}}{\sigma_{\mathrm{LO}}}(m_{t\bar{t}} < 2M_t + 100\ \mathrm{GeV}) = (-3.190 + 1.96 g_Y^2)\%, \tag{A11}$$

$$\frac{\delta\sigma_{\mathrm{EW}}^{14\,\mathrm{TeV}}}{\sigma_{\mathrm{LO}}}(m_{t\bar{t}} < 2M_t + 150\ \mathrm{GeV}) = (-2.914 + 1.44 g_Y^2)\%. \tag{A12}$$

2. Differential distributions for the LHC operating at 13 and 14 TeV

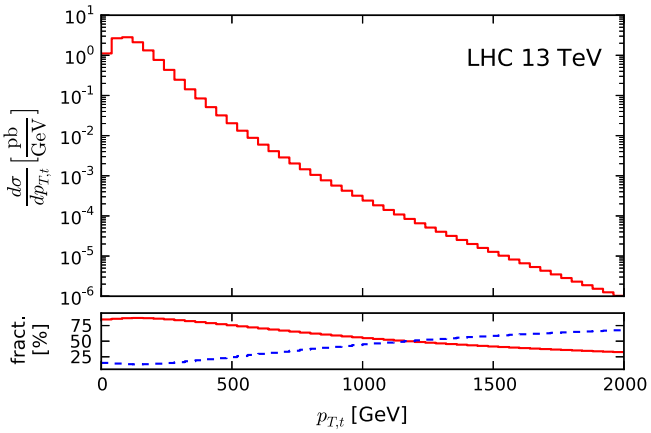

FIG. 16 (color online). Same as Fig. 6 but for 13 TeV.

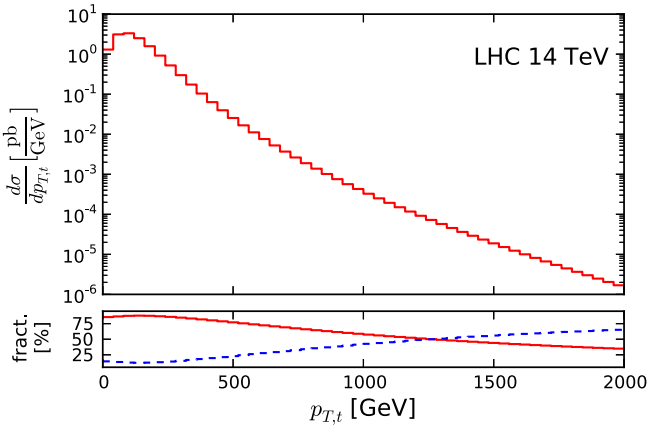

FIG. 18 (color online). Same as Fig. 6 but for 14 TeV.

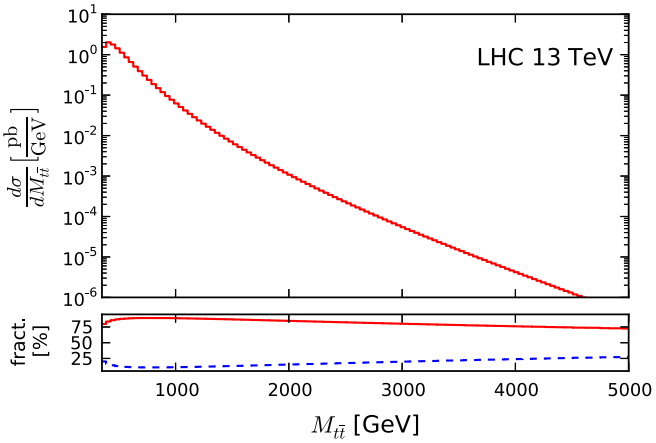

FIG. 17 (color online). Same as Fig. 7 but for 13 TeV.

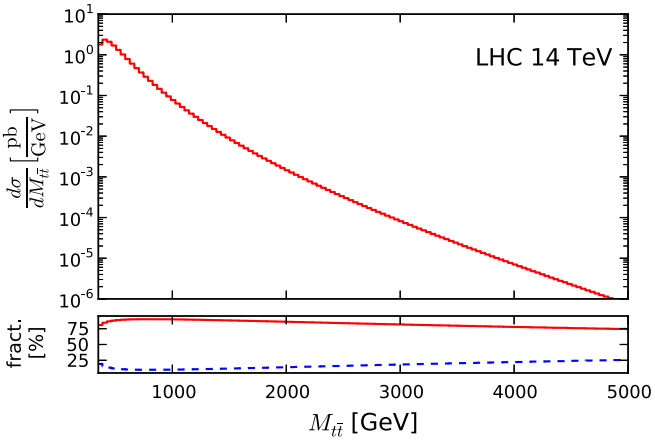

FIG. 19 (color online). Same as Fig. 7 but for 14 TeV.

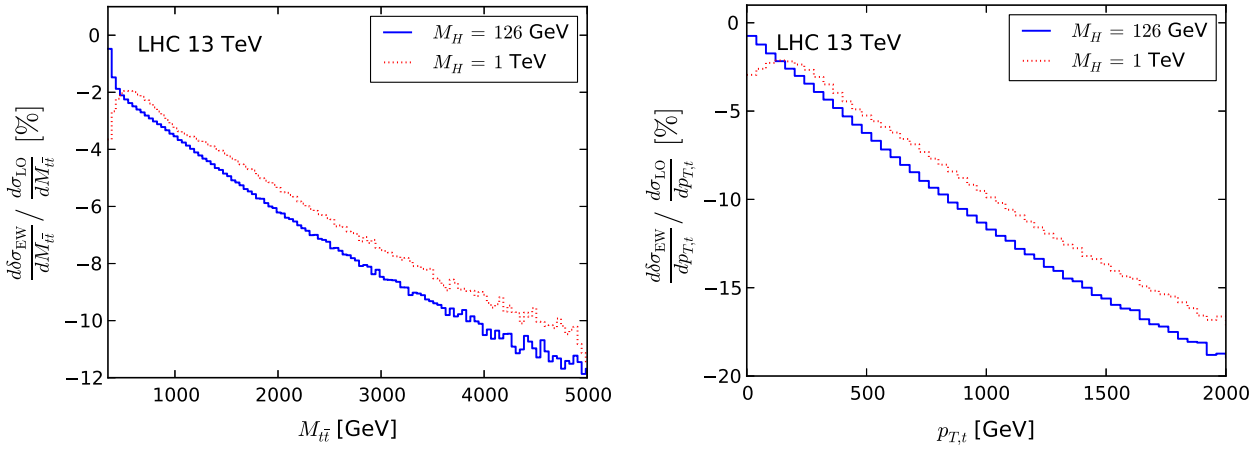

FIG. 20 (color online). Same as Fig. 12 but for 13 TeV.

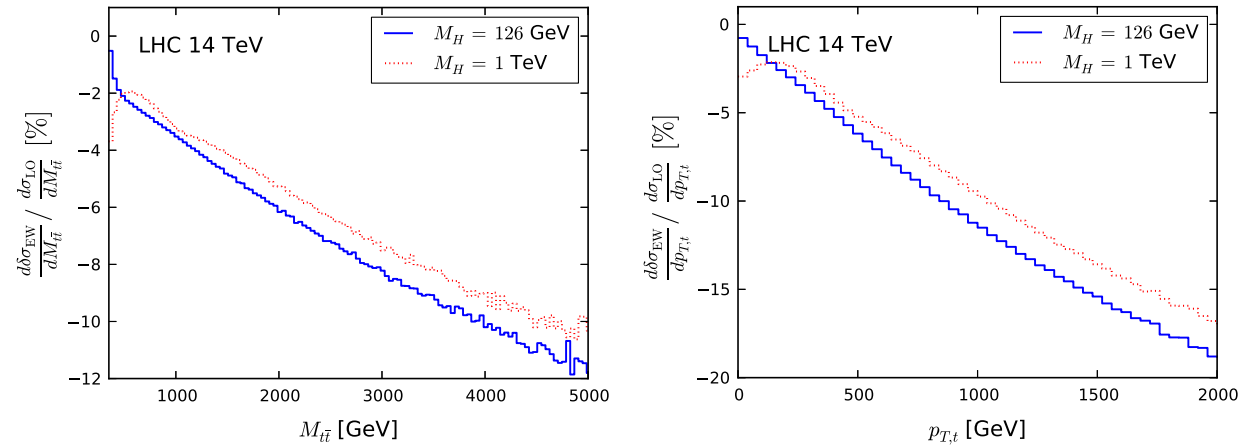

FIG. 21 (color online). Same as Fig. 12 but for 14 TeV.

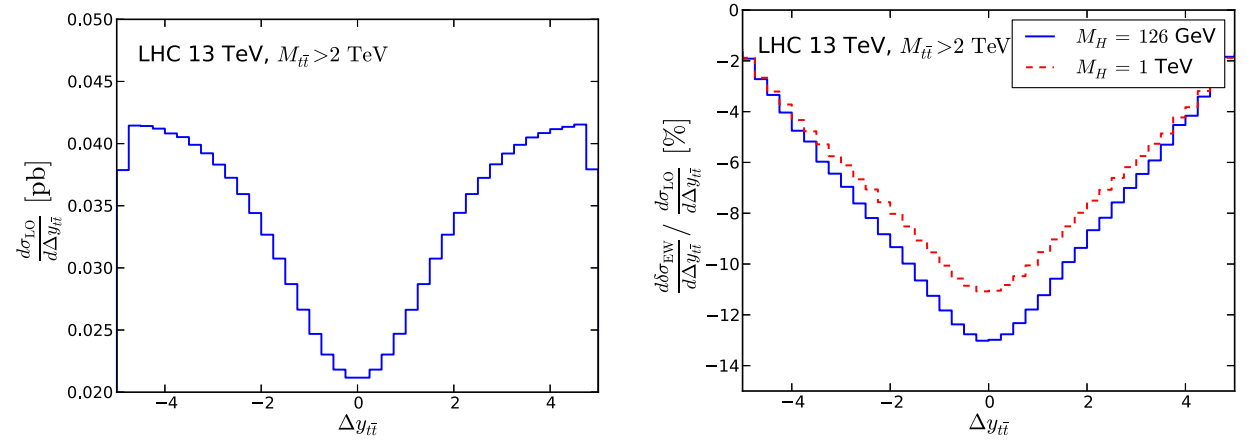

FIG. 22 (color online). Same as Fig. 13 but for 13 TeV.

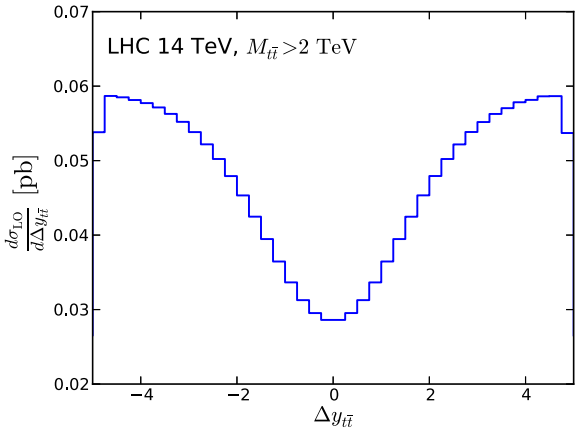

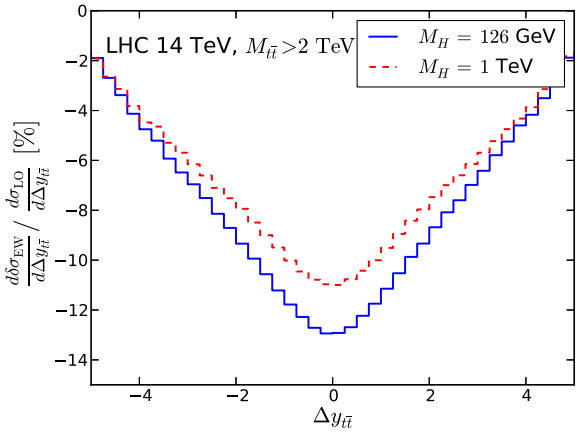

FIG. 23 (color online). Same as Fig. 13 but for 14 TeV.

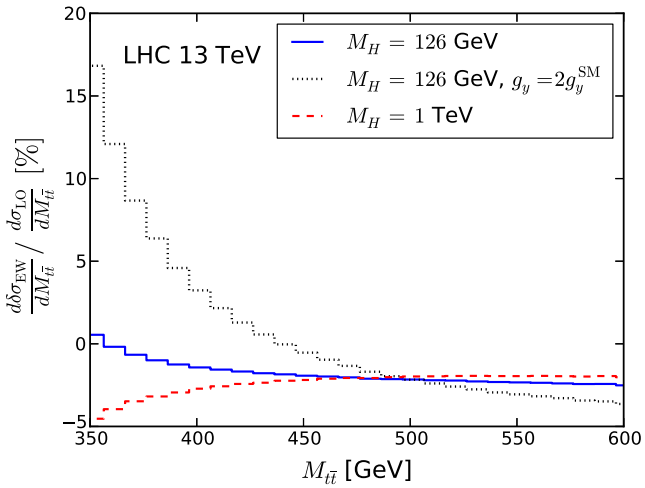

FIG. 24 (color online). Same as Fig. 14 but for 13 TeV.

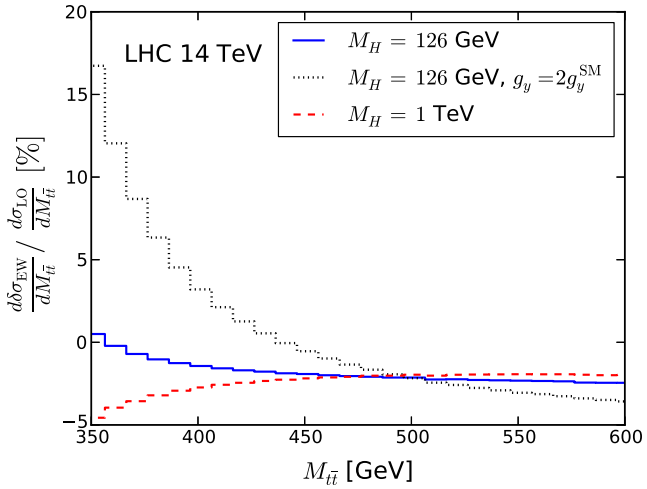

FIG. 25 (color online). Same as Fig. 14 but for 14 TeV.

[1] T. Aaltonen *et al.* (CDF and D0 Collaborations), Phys. Rev. D **86**, 092003 (2012).
[2] Tevatron Electroweak Working Group, D0 Note 6363.
[3] S. Moch and P. Uwer, Phys. Rev. D **78**, 034003 (2008).
[4] M. Aliev, H. Lacker, U. Langenfeld, S. Moch, P. Uwer, and M. Wiedermann, Comput. Phys. Commun. **182**, 1034 (2011).
[5] S. Moch, P. Uwer, and A. Vogt, Phys. Lett. B **714**, 48 (2012).
[6] M. Cacciari, M. Czakon, M. Mangano, A. Mitov, and P. Nason, Phys. Lett. B **710**, 612 (2012).
[7] P. Baernreuther, M. Czakon, and A. Mitov, Phys. Rev. Lett. **109**, 132001 (2012).
[8] M. Czakon and A. Mitov, J. High Energy Phys. 12 (2012) 054.
[9] M. Czakon and A. Mitov, J. High Energy Phys. 01 (2013) 080.
[10] M. Czakon, P. Fiedler, and A. Mitov, Phys. Rev. Lett. **110**, 252004 (2013).
[11] V. Ahrens, A. Ferroglia, M. Neubert, B. D. Pecjak, and L. L. Yang, Phys. Lett. B **703**, 135 (2011).
[12] N. Kidonakis and B. D. Pecjak, Eur. Phys. J. C **72**, 2084 (2012).
[13] N. Kidonakis and R. Vogt, Phys. Rev. D **78**, 074005 (2008).
[14] M. Beneke, P. Falgari, S. Klein, J. Piclum, C. Schwinn, M. Ubiali, and F. Yan, J. High Energy Phys. 07 (2012) 194.

[15] G. Aad *et al.* (ATLAS Collaboration), Eur. Phys. J. C **73**, 2328 (2013).
[16] G. Aad *et al.* (ATLAS Collaboration), Phys. Lett. B **717**, 89 (2012).
[17] S. Chatrchyan *et al.* (CMS Collaboration), Phys. Lett. B **720**, 83 (2013).
[18] S. Chatrchyan *et al.* (CMS Collaboration), J. High Energy Phys. 02 (2014) 024.
[19] V. Khachatryan *et al.* (CMS Collaboration), Phys. Lett. B **739**, 23 (2014).
[20] S. Chatrchyan *et al.* (CMS Collaboration), J. High Energy Phys. 05 (2013) 065.
[21] S. Chatrchyan *et al.* (CMS Collaboration), Eur. Phys. J. C **73**, 2386 (2013).
[22] G. Aad *et al.* (ATLAS Collaboration), J. High Energy Phys. 01 (2013) 116.
[23] S. Chatrchyan *et al.* (CMS Collaboration), Phys. Rev. D **87**, 072002 (2013).
[24] S. Chatrchyan *et al.* (CMS Collaboration), Eur. Phys. J. C **73**, 2339 (2013).
[25] S. Chatrchyan *et al.* (CMS Collaboration), J. High Energy Phys. 12 (2012) 015.
[26] G. Aad *et al.* (ATLAS Collaboration), Phys. Rev. D **88**, 012004 (2013).
[27] V. M. Abazov *et al.* (D0 Collaboration), Phys. Rev. D **87**, 011103 (2013).
[28] V. M. Abazov *et al.* (D0 Collaboration), Phys. Rev. D **84**, 112005 (2011).
[29] T. Aaltonen *et al.* (CDF Collaboration), Phys. Rev. D **87**, 092002 (2013).
[30] T. Aaltonen *et al.* (CDF Collaboration), Phys. Rev. D **83**, 112003 (2011).
[31] J. H. Kühn and G. Rodrigo, Phys. Rev. Lett. **81**, 49 (1998).
[32] J. H. Kühn and G. Rodrigo, Phys. Rev. D **59**, 054017 (1999).
[33] L. G. Almeida, G. F. Sterman, and W. Vogelsang, Phys. Rev. D **78**, 014008 (2008).
[34] V. Ahrens, A. Ferroglia, M. Neubert, B. D. Pecjak, and L. L. Yang, Phys. Rev. D **84**, 074004 (2011).
[35] W. Hollik and D. Pagani, Phys. Rev. D **84**, 093003 (2011).
[36] J. H. Kühn and G. Rodrigo, J. High Energy Phys. 01 (2012) 063.
[37] W. Bernreuther and Z.-G. Si, Phys. Rev. D **86**, 034026 (2012).
[38] ATLAS Collaboration, Report No. ATLAS-CONF-2012-095.
[39] ATLAS, CDF, CMS, and D0 Collaborations, arXiv:1403.4427.
[40] W. Beenakker, A. Denner, W. Hollik, R. Mertig, T. Sack, and D. Wackeroth, Nucl. Phys. **B411**, 343 (1994).
[41] J. H. Kühn, A. Scharf, and P. Uwer, Eur. Phys. J. C **45**, 139 (2006).
[42] W. Bernreuther, M. Fuecker, and Z. G. Si, Phys. Lett. B **633**, 54 (2006).
[43] W. Bernreuther, M. Fuecker, and Z.-G. Si, Phys. Rev. D **74**, 113005 (2006).
[44] J. H. Kühn, A. Scharf, and P. Uwer, Eur. Phys. J. C **51**, 37 (2007).
[45] S. Moretti, M. R. Nolten, and D. A. Ross, Phys. Lett. B **639**, 513 (2006); **660**, 607(E) (2008).
[46] W. Hollik and M. Kollar, Phys. Rev. D **77**, 014008 (2008).
[47] A. D. Martin, W. J. Stirling, R. S. Thorne, and G. Watt, Eur. Phys. J. C **63**, 189 (2009).
[48] J. H. Kühn, A. A. Penin, and V. A. Smirnov, Eur. Phys. J. C **17**, 97 (2000).
[49] J. H. Kühn, S. Moch, A. A. Penin, and V. A. Smirnov, Nucl. Phys. **B616**, 286 (2001); **B648**, 455(E) (2003).
[50] P. Kant, O. M. Kind, T. Kintscher, T. Lohse, T. Martini, S. Mölbitz, P. Rieck, and P. Uwer, arXiv:1406.4403.
[51] S. Gieseke, T. Kasprzik, and J. H. Kühn, Eur. Phys. J. C **74**, 2988 (2014).
[52] Y. Kiyo, J. H. Kühn, S. Moch, M. Steinhauser, and P. Uwer, Eur. Phys. J. C **60**, 375 (2009).
[53] B. Grzadkowski, J. H. Kühn, P. Krawczyk, and R. G. Stuart, Nucl. Phys. **B281**, 18 (1987).
[54] M. J. Strassler and M. E. Peskin, Phys. Rev. D **43**, 1500 (1991).
[55] V. S. Fadin and O. I. Yakovlev, Yad. Fiz. **53**, 1721 (1991) [Sov. J. Nucl. Phys. **53**, 1053 (1991)].
[56] M. Jezabek and J. H. Kühn, Phys. Lett. B **316**, 360 (1993).
[57] R. Harlander, M. Jezabek, and J. H. Kühn, Acta Phys. Pol. B **27**, 1781 (1996).
[58] A. Denner, R. J. Guth, and J. H. Kuhn, Nucl. Phys. **B377**, 3 (1992).
[59] R. J. Guth and J. H. Kuhn, Nucl. Phys. **B368**, 38 (1992).
[60] F. Caola and K. Melnikov, Phys. Rev. D **88**, 054024 (2013).
[61] N. Kauer and G. Passarino, J. High Energy Phys. 08 (2012) 116.
[62] V. Khachatryan *et al.* (CMS Collaboration), Phys. Lett. B **736**, 64 (2014).
[63] ATLAS Collaboration, Report No. ATLAS-CONF-2014-042.
[64] G. Aad *et al.* (ATLAS Collaboration), Phys. Lett. B **716**, 1 (2012).
[65] S. Chatrchyan *et al.* (CMS Collaboration), Phys. Lett. B **716**, 30 (2012).